electronics

MDPI

Article

Control and Stability Analysis of the *LCL*-Type Grid-Connected Converter without Phase-Locked Loop under Weak Grid Conditions

Lingling Xie, Sencai Zeng *, Jinbao Liu, Zhao Zhang and Junyi Yao

School of Electrical Engineering, Guangxi University, Nanning 530004, China
* Correspondence: zsc20123@163.com

Abstract: The stability and dynamic performance of the grid-connected converter is greatly affected by the coupling between the phase-locked loop (PLL) and the current loop control under weak grid conditions. The traditional control strategies use PLL to obtain the frequency and phase of the grid, which ignore the influence of the PLL and cannot adapt to weak grid conditions. To address this problem, the control and stability of the *LCL*-Type grid connected converter without PLL under weak grid conditions are studied in-depth in this paper. Firstly, the digital controlled model of the *LCL*-Type grid-connected converter with capacitor-current feedback active damping is established, and the stability of the system is analyzed. Then, a control strategy without PLL is proposed. The proposed strategy decomposes the grid voltage signal into instantaneous active and instantaneous reactive components through the $\alpha\beta$ frame, which can realize the independent control of active and reactive current by simple calculation. The obtained results show that the strategy avoids the influence of the PLL on the inner loop current, and has the advantages of strong stability and anti-interference ability under weak grid conditions. Finally, simulation and experiment results are provided to verify the validity of theoretical analysis.

Keywords: grid-connected converter; weak grid conditions; phase-locked loop; $\alpha\beta$ frame; system stability

check for updates

Citation: Xie, L.; Zeng, S.; Liu, J.; Zhang, Z.; Yao, J. Control and Stability Analysis of the *LCL*-Type Grid-Connected Converter without Phase-Locked Loop under Weak Grid Conditions. *Electronics* **2022**, *11*, 3322. https://doi.org/10.3390/electronics11203322

Academic Editor: Gabriel Garcerá

Received: 21 September 2022
Accepted: 11 October 2022
Published: 14 October 2022

Publisher's Note: MDPI stays neutral with regard to jurisdictional claims in published maps and institutional affiliations.

Copyright: © 2022 by the authors. Licensee MDPI, Basel, Switzerland. This article is an open access article distributed under the terms and conditions of the Creative Commons Attribution (CC BY) license (https://creativecommons.org/licenses/by/4.0/).

1. Introduction

Renewable energy has gradually become a global deployment direction in energy strategy because of its clean and renewable characteristics [1]. Due to the influences of resource distribution and climatic environment, renewable energy generation systems are often located in areas with weak grid structure, which can easily form a weak grid at the end of the connection [2]. When the conventional grid is integrated with a large number of renewable energy devices, the impedance of the grid will rise and the voltage at the point of common coupling (PCC) will be disturbed [3]. The control strategy under ideal grid conditions may cause a reduction in system stability and even trigger system oscillations when applied directly under weak grid conditions.

Real-time synchronization of the grid phase is required to ensure the power quality of grid-connected power generation systems. The phase-locked loop (PLL) is commonly used to implement phase-locked function to obtain frequency and phase information about the grid [4]. The influence of the PLL on the stability of the grid-connected converter can be ignored when the grid impedance is negligible in strong grid conditions. However, the grid impedance can greatly affect the voltage at the coupling point under weak grid conditions. In weak grid conditions, PLL will produce a perturbed output signal due to its own nonlinear impedance [5]. The PLL not only affects the voltage at PCC, but also couples with the current control loop. Therefore, it significantly decreases the power quality of grid-connected converters. In order to solve the instability problems caused by PLL, control methods involving adding feedforward or feedback terms at the current control loop have been proposed, such as output impedance reshaping methods [6] and small signal disturbance compensation control [7]. Based on these strategies, the current harmonics are reduced, but the complexity of the control system is still increased, and the accuracy depends on the operating point of the system. In [8], the PLL is modified by introducing a complex phase angle vector, which eliminates the frequency coupling term caused by the PLL. An improved parameter tuning method was proposed in [9] to mitigate the negative effects of PLL in weak grids. Although these strategies improved the power quality, it is still difficult to guarantee the inverter stability under weak grid conditions [10]. Furthermore, the complex trigonometric operation and coordinate transformation in the PLL increase the computational burden and reduce transient response time [11].

In recent years, some control strategies without PLL have been proposed to solve the instability problem caused by PLL [12–15]. In [12], a model predictive direct power control strategy was proposed to optimize the switching frequency of the grid-connected inverter. Nevertheless, the switching frequency in this strategy varies with the power output of the grid-connected converter and injects broadband harmonics into the grid. Thus, a new filter design is required to eliminate these harmonics. The power-synchronization control method proposed in [13] greatly improves the system control performance. However, its control structure does not match the industry standard vector control strategy, i.e., the over-current protection inherent in the standard vector control scheme is lost. A direct power control method is proposed in [14], but its calculation of the command current requires an additional set of coordinate transformations. In [15], a current compensation control strategy without PLL is proposed. The control strategies mentioned above are all applied under strong power grid conditions, ignoring the effect of grid impedance.

The objective of this paper is to analyze the control and stability of the *LCL*-Type grid-connected converter without PLL under weak grid conditions. The strategy without PLL decomposes the voltage signal into instantaneous active and instantaneous reactive components through the $\alpha\beta$ frame, which can realize the independent control of active and reactive current. This paper is organized as follows. The development of the model of a single-phase *LCL*-Type grid-connected converter is established in Section 2. In Section 3, a control strategy without PLL is proposed based on $\alpha\beta$ frames. Then, the stability criterion of the system under weak grid conditions is derived in Section 4. In Section 5, the simulations in Matlab are conducted, an experimental platform is established, and the results obtained from simulation and experiment are given. Finally, conclusions are drawn in Section 6.

2. Model of a Single-Phase *LCL*-Type Grid-Connected Converter

Figure 1 shows a block diagram of a single-phase *LCL*-type grid-connected converter without PLL in weak grid conditions. The *LCL* filter consists of a converter-side inductor L_1, a filter capacitor C, and a grid side inductor L_2. C_1 is the capacitor and load resistance of the DC-side. Power switches T_1~T_4 and their antiparallel diodes form the converter bridge. Z_g is the grid impedance at the point of common coupling (PCC). U_g and U_{inv} represent the grid voltage and input of the converter bridge. H_1 and H_2 are the feedback coefficients of the capacitor and grid currents, respectively. $G_i(s)$ is the grid current regulator transfer function.

The digital control methods have a one-beat hysteresis delay. A zero-order holder (ZOH) and a one-beat hysteresis link are added to the grid-connected converter model.

The transfer function of the ZOH is:

$$G_h(s) = 1 - e^{-sT_s}/s \approx T_s e^{-0.5sT_s} \tag{1}$$

The double closed-loop control structure on the voltage and current is used. The external DC voltage loop uses a PI controller to regulate the DC side voltage, which provides stable output for the d-axis reference current amplitude i_d^*, and the q-axis reference current i_q^* is given directly. The given reference current i_s^* is obtained by i_d^* and i_q^*. According to the requirements of the electrical energy conversion, the inner loop current *S*-domain model of the grid-connected current is established as shown in Figure 2.

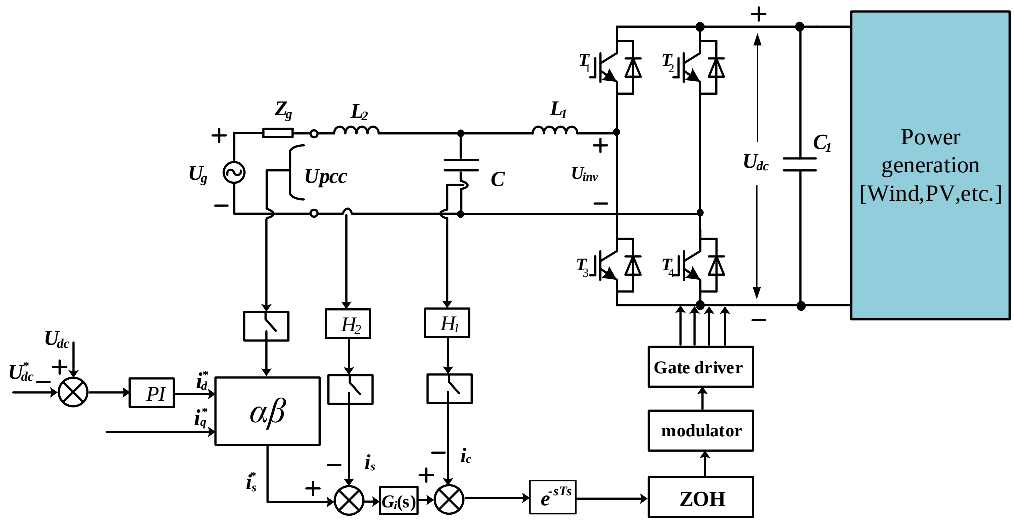

Figure 1. Structure diagram of *LCL*-Type grid-connected converter without PLL in weak gird conditions.

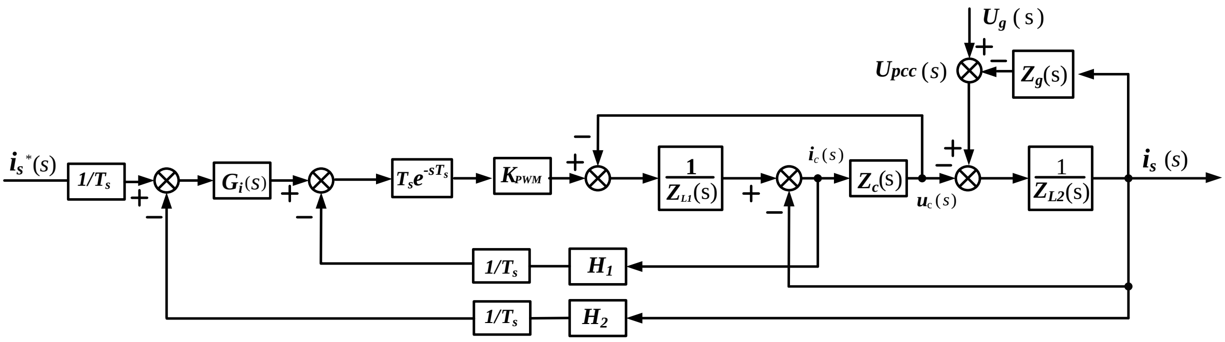

Figure 2. S-domain model of grid-connected current.

In Figure 2, $1/T_s$ is the transfer function of the sampling switch [16], and $K_{PWM} = U^{*}_{dc}/U_{tri}$, U_{tri} represents the amplitude of the triangular carrier wave. The Simplified *S*-domain model is shown in Figure 3 [17].

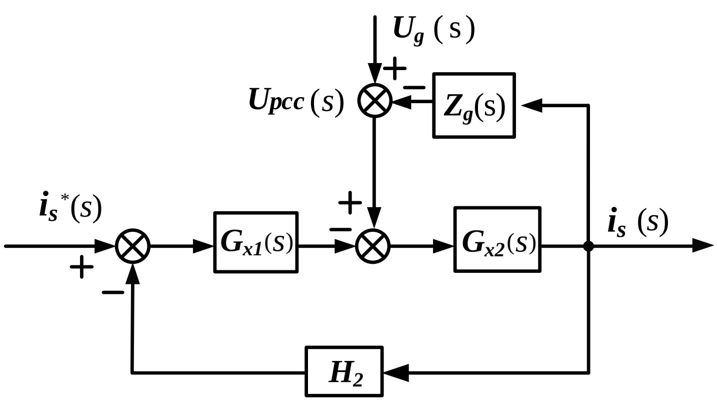

Figure 3. Simplified S-domain model of grid-connected current.

In Figure 3,

$$G_{x1} = \frac{G_i Z_C G_Z K_{PWM}}{Z_{L1} + H_1 K_{PWM} G_Z + Z_C} \quad (2)$$

$$G_{x2} = \frac{Z_{L1} + H_1 K_{PWM} G_Z + Z_C}{Z_{L2}(Z_{L1} + H_1 K_{PWM} G_Z + Z_C) + Z_{L1} Z_C} \quad (3)$$

$$G_Z = \frac{1}{T_s} e^{-sT_s} G_h \approx e^{-1.5sT_s} \tag{4}$$

where $Z_{L1} = sL_1; Z_{L2} = sL_2; Z_C = 1/sC$.

The loop gain of the grid-connected current can be obtained as the following:

$$T_{ig} = G_{x1} G_{x2} H_2 \tag{5}$$

Thus, the grid connection current can be deduced as:

$$i_s = \frac{G_{x2}}{1 + T_{ig}} U_{PCC} - \frac{1}{H_2} \frac{T_{ig}}{1 + T_{ig}} i_s^* \tag{6}$$

3. Control Strategies for Grid Currents

One of the most popular phase-locked methods is synchronous reference frame PLL (SRF-PLL) [18,19]. The control block diagram of the SRF-PLL is shown in Figure 4. In Figure 4, the AC voltage component with phase lag of 90° at the U_{PCC} is generated by the OSG (Orthogonal Signal Generators) module. The orthogonal signals U_α and U_β are transformed into the voltages U_d and U_q in the rotating frame system [20].

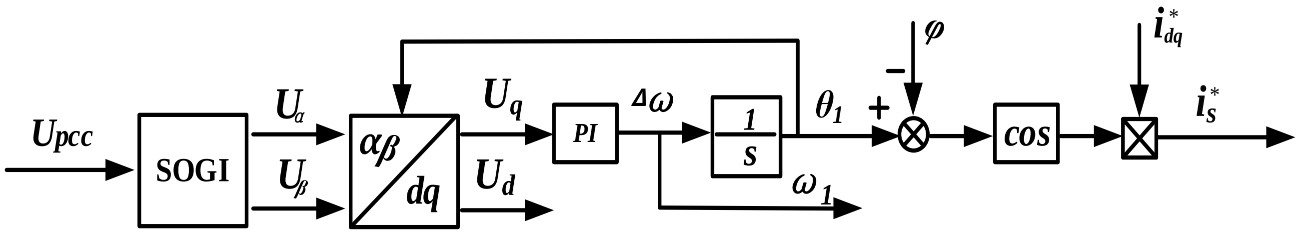

Figure 4. Phase locked loop control model.

The characteristic transfer functions of SOGI are given by:

$$\begin{cases} D(s) = \frac{U_\alpha}{U_{PCC}} = \frac{k\omega_0 s}{s^2 + k\omega_0 s + \omega_0^2} \\ Q(s) = \frac{U_\beta}{U_{PCC}} = \frac{k\omega_0^2}{s^2 + k\omega_0 s + \omega_0^2} \end{cases} \tag{7}$$

where ω_0 and k are set as the resonance frequency and damping factor of the SOGI. It can be seen from Figure 4 that the reference current i_s^* is not an independent variable, and its expression is:

$$i_s^* = i_{dq}^* T_{\mathrm{PLL}} D(s) U_{PCC} \tag{8}$$

where T_{PLL} is the transfer function of the PLL, i_{dq}^* is the active and reactive reference current.

From the above discussion, one conclusion that can be drawn is that the stability of the current loop is affected by the PLL. This means that the traditional control strategy will become more complicated. Thus, it is difficult to guarantee its stability.

To address this problem, a control strategy without PLL is proposed. Considering that single-phase systems lack a degree of freedom, the control strategy based on the $\alpha\beta$ frame is more compact than the method based on the dq frame. The $\alpha\beta$ frame control strategy with voltage sampling signals can achieve independent control of active and reactive current by decomposing the voltage signal into instantaneous active and instantaneous reactive components. The orthogonal signal is generated by delaying the original single-phase signal by $T/4$, where T is the grid fundamental period [21]. The control model is shown in Figure 5.

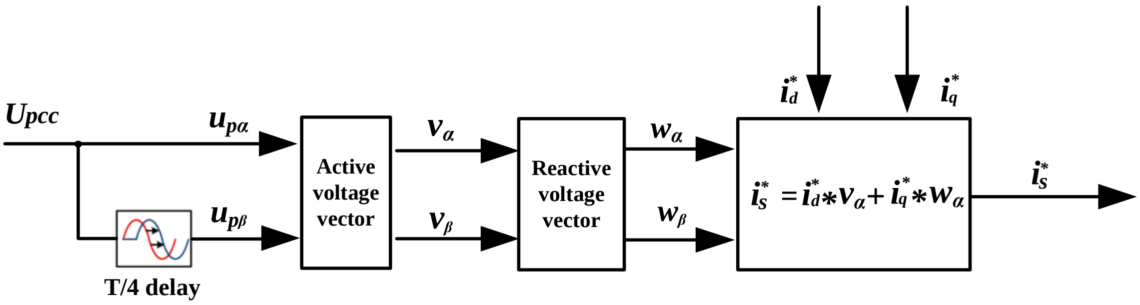

Figure 5. Control model in $\alpha\beta$ frames.

Assuming that the grid voltage is clean and undistorted, the command current in $\alpha\beta$ frames based on the grid voltage without PLL is calculated as:

$$\begin{bmatrix} i_{s\alpha}^* \\ i_{s\beta}^* \end{bmatrix} = \begin{bmatrix} v_\alpha & w_\alpha \\ v_\beta & w_\beta \end{bmatrix} \begin{bmatrix} i_d^* \\ i_q^* \end{bmatrix} \tag{9}$$

where $v = (v_\alpha, v_\beta)^T$ is the active voltage unit vector in $\alpha\beta$ frames, $w = (w_\alpha, w_\beta)^T$ is the reactive voltage unit vector in $\alpha\beta$ frames. According to instantaneous power theory, the mathematical relationship between v and w is:

$$\begin{bmatrix} v_\alpha \\ v_\beta \end{bmatrix} = \frac{1}{|u_p|} \begin{bmatrix} u_{p\alpha} \\ u_{p\beta} \end{bmatrix} \tag{10}$$

$$\begin{bmatrix} w_\alpha \\ w_\beta \end{bmatrix} = \begin{bmatrix} 0 & 1 \\ -1 & 0 \end{bmatrix} \begin{bmatrix} v_\alpha \\ v_\beta \end{bmatrix} \tag{11}$$

Define $u_p = (u_{p\alpha}, u_{p\beta})^T$ as the voltage vector in the $\alpha\beta$ frame system, in which $u_{p\alpha}$ is the same as U_{PCC}. $|u_p|$ represents its amplitude, which can be calculated from the amplitudes of u_α and u_β:

$$|u_p| = \sqrt{u_{p\alpha}^2 + u_{p\beta}^2} \tag{12}$$

Thus, the grid reference current can be quickly obtained from (9)~(12) as follows:

$$i_s^* = i_{s\alpha}^* = i_d^* v_\alpha + i_q^* w_\alpha \tag{13}$$

As seen in Equation (13), the reference current i_s^* can be controlled independently by changing the active currents reference i_d^* and reactive currents reference i_q^*. When i_q^* = 0, the reference current i_s^* and the voltage U_{PCC} are in the same frequency and phase, the phase lock can be realized without PLL. When i_*^d = 0, the phase difference between reference current and the voltage U_{PCC} is 90°.

4. Stability Analysis

The grid-connected converter and the grid can be seen as a cascaded system with the grid existing impedance. Thus, Equation (6) can be rewritten as follows:

$$i_s = \frac{U_{PCC}}{Z_o} - i_1 \tag{14}$$

where i_1 and Z_o are the equivalent ideal current source and output impedance of the grid-connected converter, respectively:

$$Z_o = \frac{1 + T_{ig}}{G_{x2}} \tag{15}$$

$$i_1 = \frac{1}{H_2} \frac{T_{ig}}{1 + T_{ig}} i_s^* \tag{16}$$

The equivalent circuit of a single-phase *LCL*-type grid-connected converter connected to a weak grid can be obtained according to Equation (14), as shown in Figure 6. $i_s(s)$ represents the grid connection current and $Z_g(s)$ is the grid impedance.

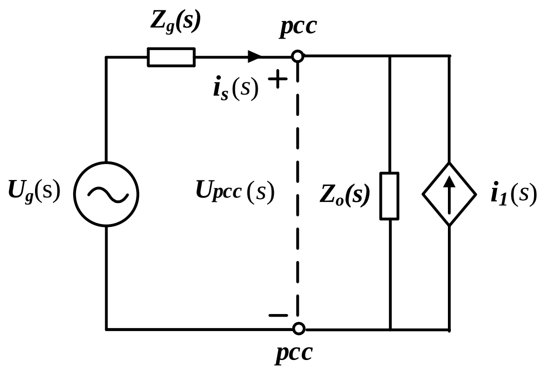

Figure 6. Equivalent circuit of grid-connected system.

The expression for the grid connection current can be obtained as:

$$\begin{aligned} i_s(s) &= \tfrac{1}{Z_o(s)+Z_g(s)} U_g(s) - \tfrac{Z_o(s)}{Z_o(s)+Z_g(s)} i_1(s) \\ &= N(s)\left(\tfrac{U_g(s)}{Z_o(s)} - i_1(s)\right) \end{aligned} \tag{17}$$

where:

$$N(s) = \frac{1}{1 + Z_g(s)/Z_o(s)} \tag{18}$$

It can be seen that the stability of the system depends on $[U_g(s)/Z_o(s) - i_1(s)]$ and $N(s)$. When Z_g = 0, the grid-connected converter is a stable system, $[U_g(s)/Z_o(s) - i_1(s)]$ does not contain a right-plane pole. For $N(s)$, it is required that $[Z_g(s)/Z_o(s)]$ satisfies the Nyquist stability criterion. Based on the above derivation, the stability of the grid-connected converter under weak grid conditions needs to satisfy the following two conditions:

(1) The grid-connected converter is stable when Z_g = 0;
(2) The impedance ratio $Z_g(s)/Z_o(s)$ satisfies the Nyquist stability criterion.

Condition (1) can be satisfied only by correcting the loop gain T_{ig}. Condition (2) requires $Z_g(s)/Z_o(s)$ to have a certain phase margin (*PM*) at 0 dB, which can be calculated as:

$$PM = \left| -180^\circ + \arg[Z_g(j2\pi f_i)] - \arg[Z_o(j2\pi f_i)] \right| \tag{19}$$

where f_i is the crossover frequency, and the grid impedance Z_g is generally resistive inductive [22]. Considering the worst case, the grid impedance is set as pure inductance. Thus, Equation (19) can be simplified to:

$$PM = 90^\circ + \arg[Z_o(j2\pi f_i)] \tag{20}$$

It must be ensured that *PM* is greater than 0°, so that the system is stable. It is necessary to make sure that the corresponding phase of Z_o at each intercept frequency is greater than −90° when the amplitudes of Z_g and Z_o intersect multiple times. When the grid impedance changes, using this criterion to analyze the stability of the grid-connected converter, there is no need to re-model the grid-connected converter.

5. Simulation and Experimental Verification

5.1. Simulation

Simulation was carried out in the MATLAB/Simulink software. The parameters are shown in Table 1. The variation range of the grid impedance can be calculated from the short circuit ratio (SCR) at the PCC [23]. According to the definition of SCR, the maximal grid impedance is 1.8 mH.

Table 1. Parameters of system.

Parameters	Values
U_g	80 V
U_{dc}^*	150 V
f_o	50 Hz
f_s	20 kHz
f_{sw}	10 kHz
L_1	300 µH
C	10 µF
L_2	180 µH
U_{tri}	3 V
H_2	0.14
C_1	10,000 µF
R_L	40 Ω

A PR regulator with the following transfer function is used for the current regulator:

$$G_i(s) = K_p + \frac{2K_r\omega_i s}{s + 2\omega_i s + \omega_0^2} \tag{21}$$

The system current loop gain T_{ig} can be rewritten as:

$$\begin{aligned} T_{ig}(s) &= G_{x1}(s)G_{x2}(s)H_2 \\ &= \frac{H_2 K_{PWM} G_i(s) G_Z(s)}{s^3 L_1 L_2 C + s^2 L_2 C H_1 K_{PWM} G_Z(s) + s(L_1 + L_1)} \end{aligned} \tag{22}$$

The amplitude margins GM_1 and GM_2 of the system at f_r and $f_s/6$ are:

$$GM_1 = -20\lg\left|T_{ig}(j2\pi f_r)\right| \tag{23}$$

$$GM_2 = -20\lg\left|T_{ig}(j2\pi f_s/6)\right| \tag{24}$$

According to the method proposed in [24], K_p = 0.54, K_r = 115 and the capacitor current feedback coefficient H_1 = 0.02.

The Bode diagram of the corrected grid-connected current loop gain is shown as the red solid line in Figure 7. It can be seen from Figure 7 that the phase margin PM = 51.5°, and the magnitude margins at f_r and $f_s/6$ are GM_1 = −8.21 dB and GM_2 = 3.46 dB, respectively. Therefore, the system is stable.

The Bode diagrams of Z_g and Z_o are shown in Figure 8, where the blue solid line represents Z_o and the red dotted line represents Z_g. From the Figure 8, it can be seen that the impedance crossover frequency is f_i = 1030 Hz, the phase margin of the system is PM = 55.3°. Thus, the grid-connected converter system is still stable and has good robustness. Assuming that the system parameters are K_p = 0.14, K_r = 50, H_1 = 0.01. The current loop gain is shown as the blue dotted line in Figure 7. We can see that the resonant peak is less than 0 dB, and GM_1 = 0.16 dB and GM_2 = −1.35 dB. The results violate Condition (1) in Section 4; thus, the current loop is unstable. The black dotted line in Figure 8 indicates that the PM of Z_g and Z_o at the intersection frequency is less than 0, which violates Condition (2) in Section 4, so the system will experience instability.

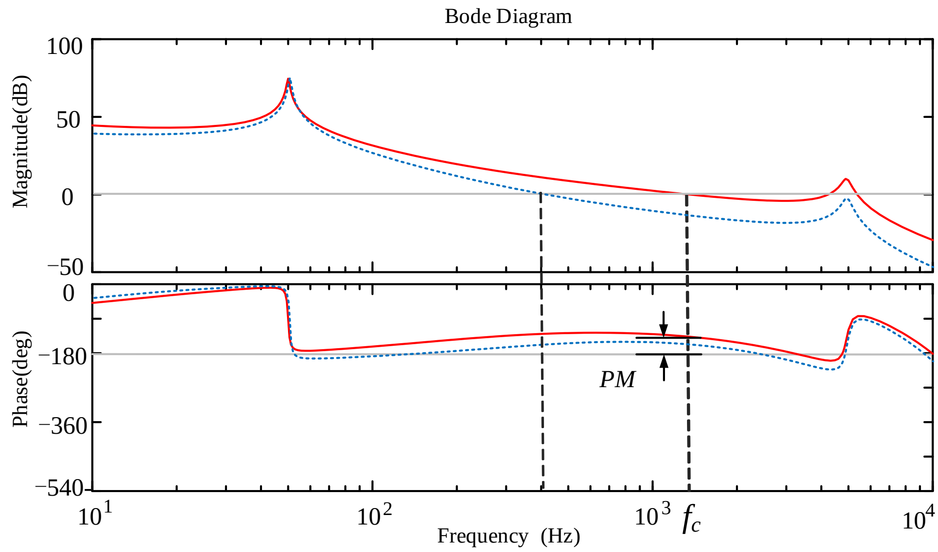

Figure 7. Bode diagram of the loop gain.

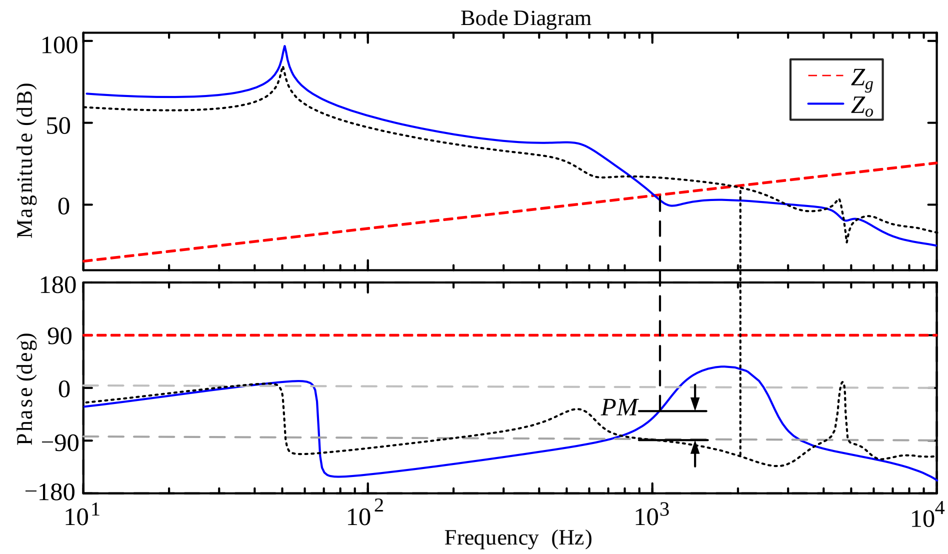

Figure 8. Bode diagram of Z_g and Z_o.

The waveforms of U_{PCC} and i_s in different conditions with Z_g =1.8 mH (corresponding to the short-circuit ratio SCR = 10) are shown in Figure 9. Figure 9a,b shows that the grid current and voltage are in the same frequency and phase without using the PLL control strategy. The grid current can track the active current reference rapidly and accurately. In addition, THD is only 0.75%. The system is stable and the power quality is good. Figure 9c, d illustrates that the grid current is able to track the inductive reactive current reference (i_q^* = 20 A) and capacitive reactive current reference (i_q^* = −20 A) in steady state. The phase difference between grid current and the voltage U_{PCC} is 90°. Therefore, the proposed strategy satisfies steady-state performance. Figure 9e,f shows that when the reactive current reference i_q^* suddenly changes from 10 A to 20 A and −10 A to −20 A, the system responds quickly, and the tracking is rapid and smooth. Figure 9g,h show that when the amplitude and phase of the voltage are suddenly changed, the tracking is rapid too. It can be seen that the system has good dynamic performance.

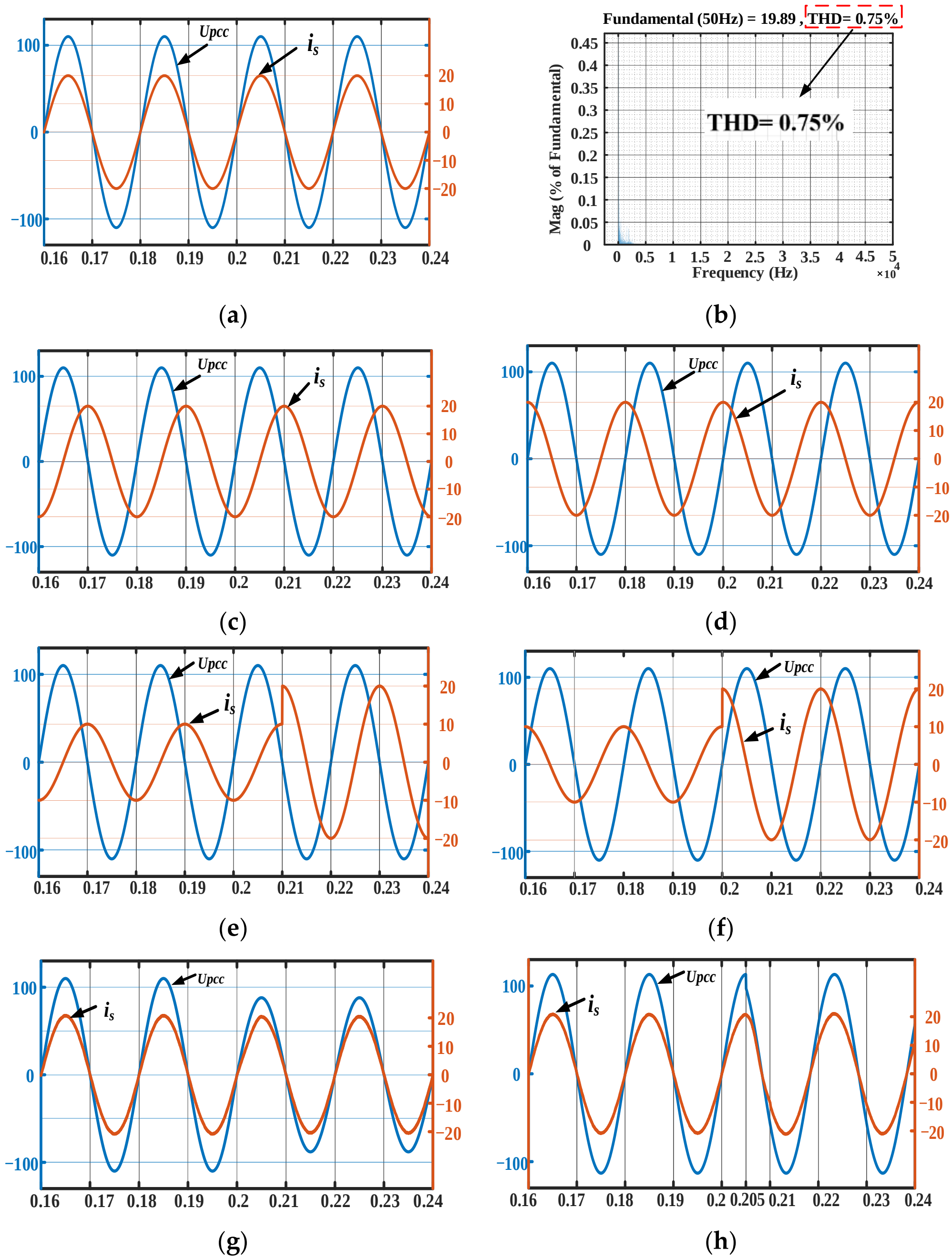

Figure 9. Waveforms of U_{PCC} and i_s. (**a**) Steady-state; (**b**) THD of grid current; (**c**) Inductive reactive current; (**d**) Capacitive reactive current; (**e**) Reactive current changes from 10 A to 20 A; (**f**) Reactive current changes from −10 A to −20 A; (**g**) U_{PCC} suddenly dropping; (**h**) The phase of U_{PCC} suddenly jumping (30°).

5.2. Experimental Verification

To further verify the effectiveness of the methods, a 1.1 kW *LCL*-type single-phase grid-connected converter was built, as shown in Figure 10. The parameters were the same as those in Table 1.

The electronic switches were Infineon IGBT module F4100R12KS4, and the DSP model was a 32-bit floating point digital signal processor TMS320F28377D. A programmable AC power supply (Chroma 6530) was used to generate sinusoidal grid voltage, and the impedance of the power grid was simulated by connecting inductor. There were four DSP built-in 16-bit ADC sampling modules, and Hall sensors were used to detect the grid voltage, grid current, and DC-side voltage signals.

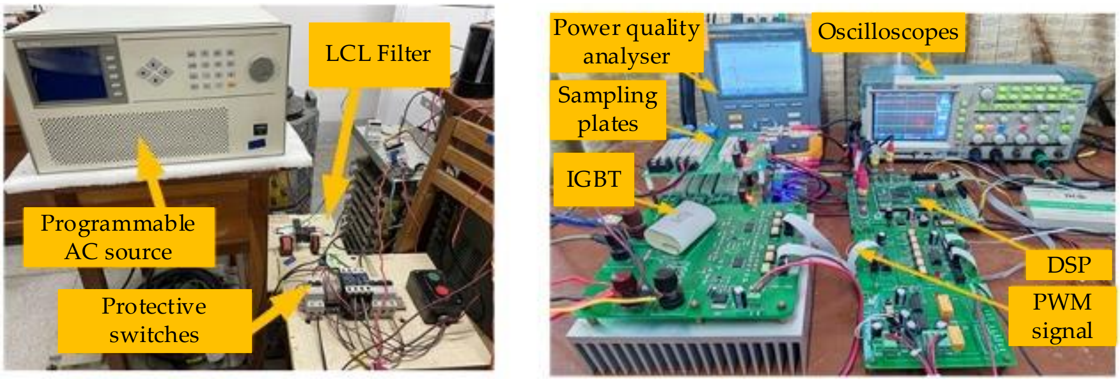

Figure 10. Experimental setup of the grid-connected converter.

Figure 11 shows the waveform of U_{PCC}, i_s and the THD of the grid current with different grid impedances Z_g.

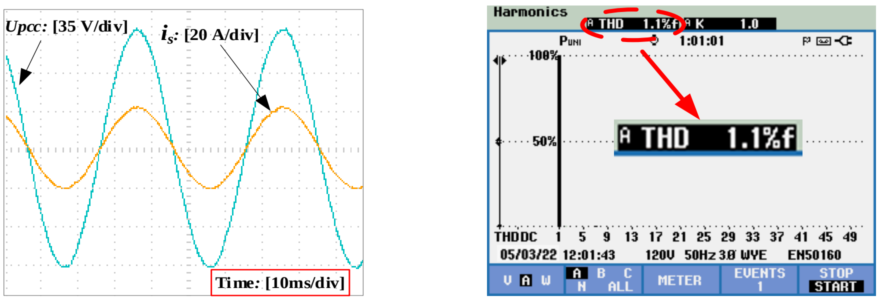

(**a**)

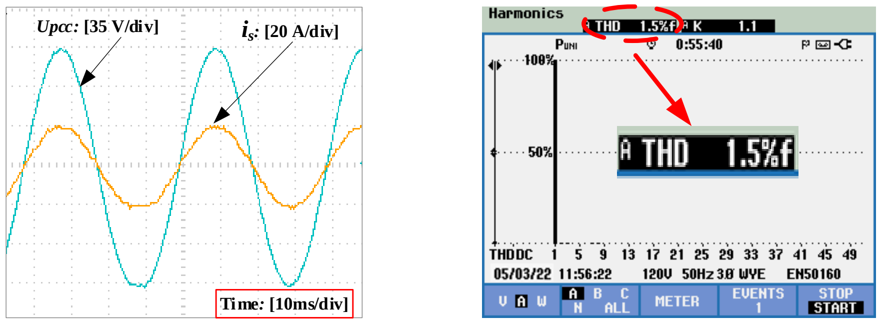

(**b**)

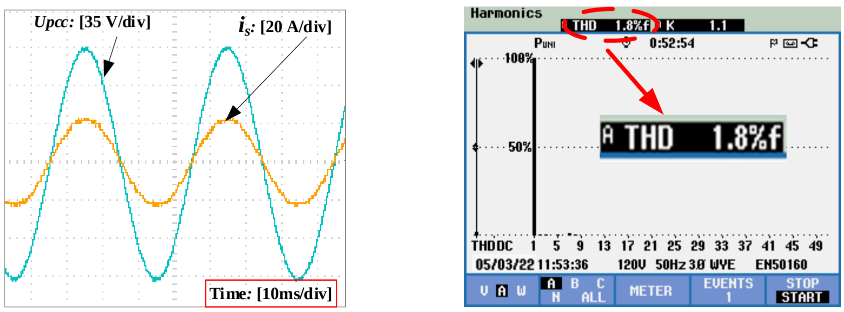

(**c**)

Figure 11. Waveform of U_{PCC}, i_s and the THD of the grid current with different Z_g. (**a**) Z_g = 0 mH; (**b**) Z_g = 0.9 mH; (**c**) Z_g = 1.8 mH.

From Figure 11a–c, we can see that the system worked stably when the grid impedance varied in the full range from 0 to 1.8 mH, and the THDs of the grid current were less than 1.8%. Table 2 shows that the third and fifth harmonic contents of the grid current were less than 1.1%. The proposed strategy was very stable under weak grid conditions.

Table 2. 3rd and 5th harmonics in all cases.

	3rd	5th
Z_g = 0 mH	0.78%	0.49%
Z_g = 0.9 mH	0.95%	0.58%
Z_g = 1.8 mH	1.06%	0.69%

Figure 12 shows the waveform of U_{PCC}, i_s and the THD of the grid current under PLL control with Z_g = 1.8 mH. It can be seen that the waveforms of the voltage and current are distorted, which indicate a poor harmonic suppression capability in the system, resulting in a large harmonic content of the grid current. The THD of the grid current is 7.3%, which is higher than the 5% defined by the electrical energy quality standard.

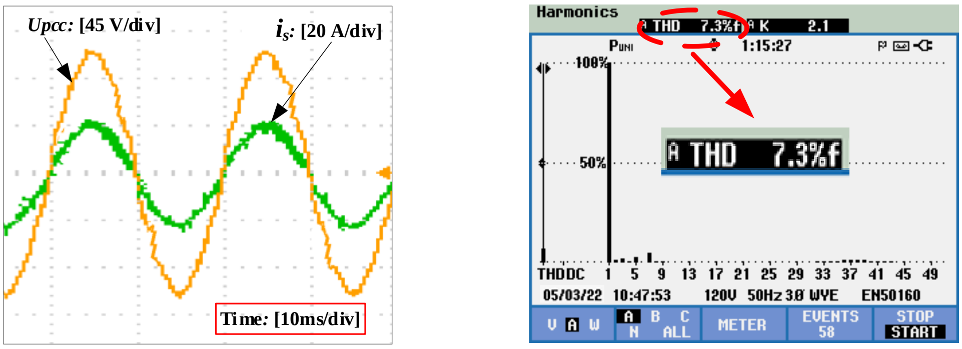

Figure 12. Waveform of U_{PCC}, i_s and the THD of the grid current under PLL control with Z_g = 1.8 mH.

Comparing Figure 11c with Figure 12, it is obvious that the proposed method could effectively adapt to weak grid conditions, and the current i_s and voltage U_{PCC} remained in the same frequency and phase. Furthermore, the proposed control method reduced the THD of the output current, increased the stability as well as the robustness of the system, and improves the power quality.

The waveforms of U_{PCC}, i_s under different control methods with Z_g = 1.8 mH are shown in Figures 13 and 14. Figure 13a,b shows that the grid current tracked the reactive current reference with smooth waveform and lower harmonic content at steady state. In Figure 14a,b, the grid current has a certain degree of distortion and poor steady-state performance. A number of burrs in the waveforms suggest that PLL affected the output impedance of the system, which had a serious impact on the stability of the inner loop current. The comparison verified that the proposed method had stronger harmonic suppression ability, so as to better realize the function of reactive power compensation.

Figures 15 and 16 show the waveforms of U_{PCC} and i_s under different controls, with the reactive current reference i_q^* changing suddenly.

Figure 15 shows that the actual current rose rapidly without any time delay or overshoot during the dynamic process under weak grid conditions. The steady-state current before and after the transient state was stable in amplitude and 90° ahead or behind the voltage in phase. Thus, the proposed control method without PLL had good steady-state and dynamic performance. In contrast, Figure 16 shows a slow transient response of the system. When the reactive current i_q^* changed suddenly, the grid current needed a delay of at least 5 ms before it was completely tracked. Obviously, the control strategy without PLL was more suitable than the PLL control strategy in weak grid conditions.

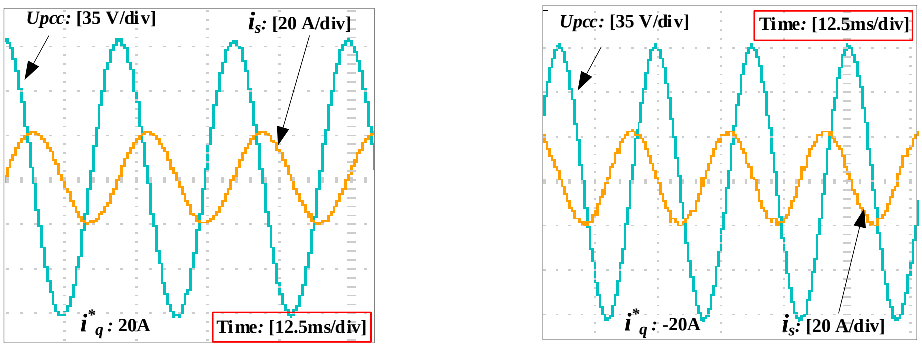

(**a**) (**b**)

Figure 13. Waveforms of U_{PCC} and i_s without PLL. (**a**) Inductive reactive current; (**b**) capacitive reactive current.

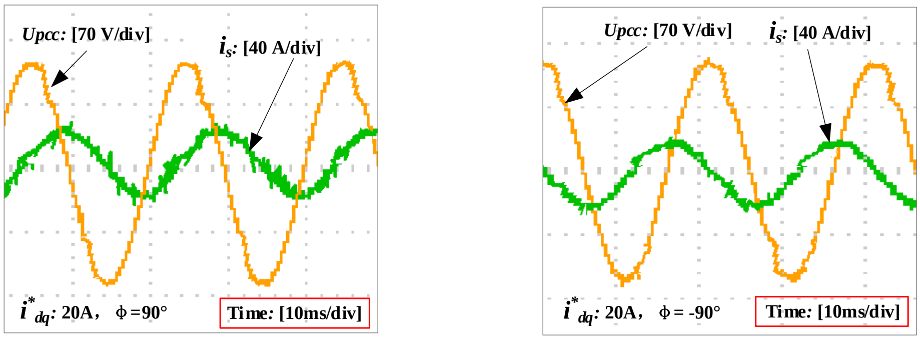

(**a**) (**b**)

Figure 14. Waveforms of U_{PCC} and i_s with PLL. (**a**) Inductive reactive current; (**b**) capacitive reactive current.

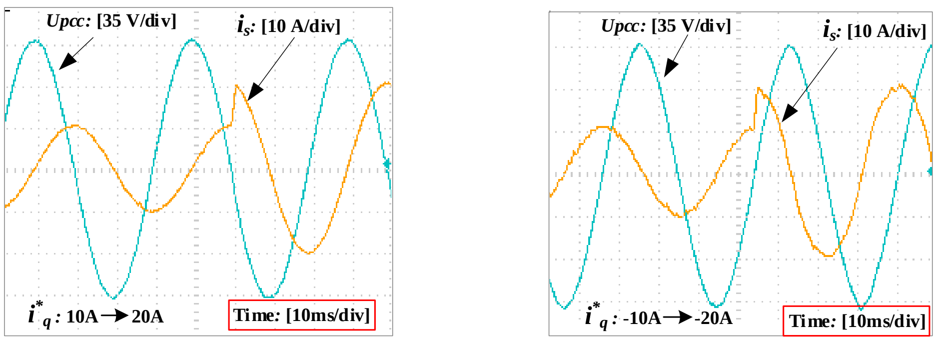

(**a**) (**b**)

Figure 15. Waveforms of U_{PCC} and i_s without PLL when Z_g = 1.8 mH. (**a**) i_q^* changes from 10 A to 20 A; (**b**) i_q^* changes from −10 A to −20 A.

The waveforms of U_{PCC} and i_s with U_{PCC} suddenly dropping from 113 V to 85 V are shown in Figure 17. It can be seen that when the grid voltage changed suddenly, the amplitude and phase of the grid current did not change. The grid current remained stable.

Figure 18 shows that when the phase of the voltage was suddenly changed at a certain moment, the tracking was rapid. The current and voltage was able to maintain the same frequency and phase after the change of phase. When $\theta = \pm 30°$, the current could track the phase in a very short time, and when a = ±60° or ±90°, the tracking process would not exceed $T/4$ (5 ms). It is shown that the proposed method is feasible under weak grid conditions.

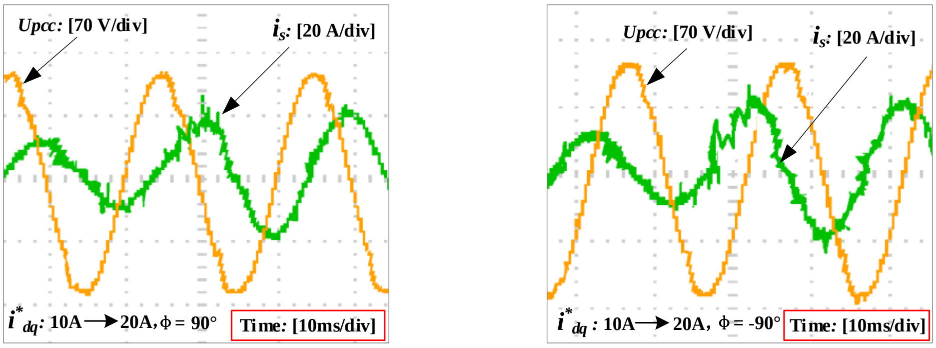

(**a**) (**b**)

Figure 16. Waveforms of U_{PCC} and i_s with PLL when Z_g = 1.8 mH. (**a**) i^*_{dq} changes from 10 A to 20 A, φ = 90°; (**b**) i^*_{dq} changes from 10 A to 20 A, φ = −90°.

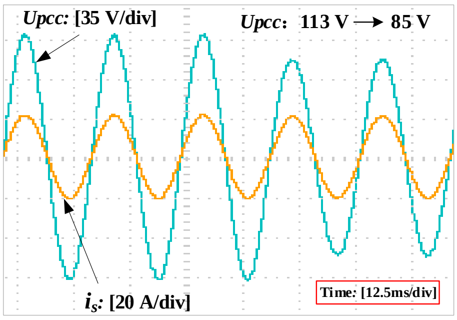

Figure 17. Waveforms of U_{PCC} and i_s with U_{PCC} suddenly dropping from 113 V to 85 V when Z_g = 1.8 mH.

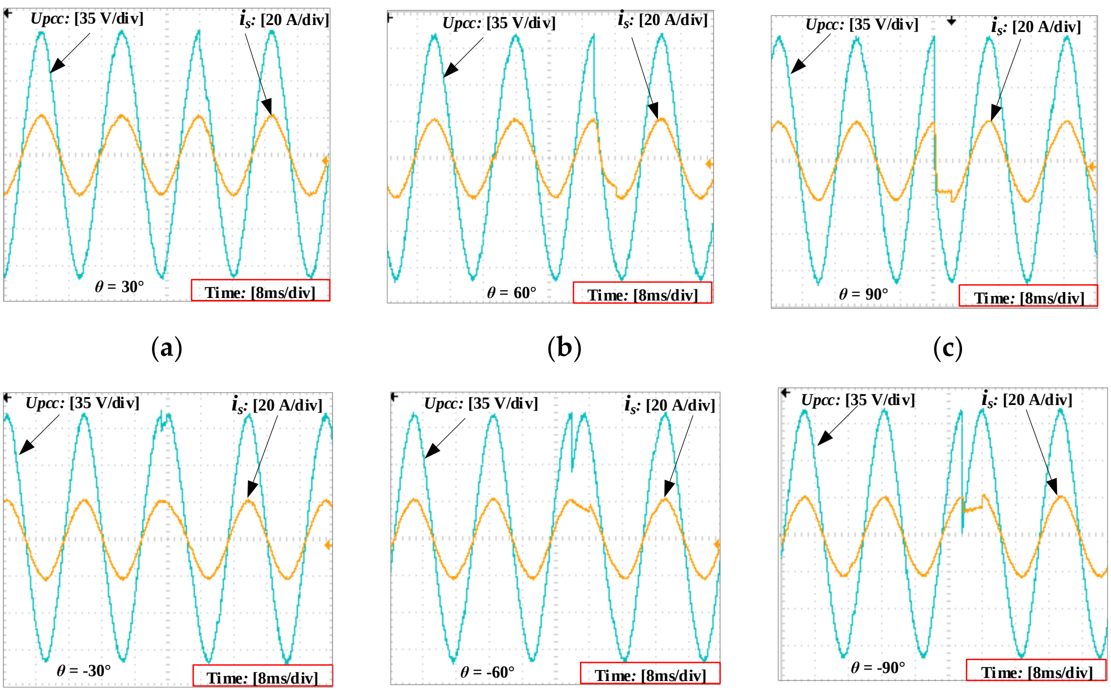

(**a**) (**b**) (**c**)

(**d**) (**e**) (**f**)

Figure 18. Waveforms of U_{PCC} and i_s with the phase of U_{PCC} suddenly jumping. (**a**) θ = 30°; (**b**) θ = 60°; (**c**) θ = 90°; (**d**) θ = −30°; (**e**) θ = −60°; (**f**) θ = −90°.

6. Conclusions

The stability of a single-phase *LCL*-Type grid-connected converter under weak grid conditions was analyzed. Two conditions for the stability of the grid-connected converter under weak grid needs to satisfy were derived. A control strategy without PLL was proposed. The strategy decomposed the voltage signal into instantaneous active and instantaneous reactive components through the $\alpha\beta$ frame, which realized the independent control of active and reactive current. Simulations and experiments were carried out. Based on the obtained results, the following conclusions can be drawn:

(1) The proposed control strategy can effectively avoid the harmonic and instability problems caused by PLL under weak grid conditions. The THD of the grid current is less than 1.8% and the third and fifth harmonic contents are less than 1.1%. Compared with the traditional control strategy, it has better steady-state performance and stronger robustness.
(2) This method does not need Park transforms and PLL, which reduces the computation and complexity and is beneficial to digital realization.
(3) When the reactive current or the grid voltage changes suddenly, the system can respond quickly, and the tracking is fast. The system has better dynamic performance.

Author Contributions: Project administration, L.X.; writing—original draft preparation, S.Z.; investigation, Z.Z. and J.L.; validation, J.Y. All authors have read and agreed to the published version of the manuscript.

Funding: This research was funded by National Natural Science Foundation of China, grant number 61861003.

Data Availability Statement: The data presented in this study are available on request from the corresponding author.

Acknowledgments: This study was supported by National Natural Science Foundation of China, grant number 61861003.

Conflicts of Interest: The authors declare no conflict of interest.

References

1. Priyadarshi, N.; Bhaskar, M.S.; Azam, F.; Singh, M.; Dhaked, D.K.; Taha, I.B.M.; Hussien, M.G. Performance Evaluation of Solar-PV-Based Non-Isolated Switched-Inductor and Switched-Capacitor High-Step-Up Cuk Converter. *Electronics* **2022**, *11*, 1381. [CrossRef]
2. Maganti, S.; Padhy, N.P. A Flexible Compensation Strategy for Weak Grid-Tied Current Controlled Converters under Unbalanced and Harmonic Conditions. In Proceedings of the 2020 IEEE International Conference on Power Electronics, Drives and Energy Systems (PEDES), Jaipur, India, 16–19 December 2020; pp. 1–5. [CrossRef]
3. Lin, P.; Zhang, C.; Wang, P.; Li, X.; Xiao, J.; Tu, P.; Hoong, C.F. A global robust output regulation method for grid-connected inverter with LCL filter in weak grid condition. In Proceedings of the 2017 12th IEEE Conference on Industrial Electronics and Applications (ICIEA), Siem Reap, Cambodia, 18–20 June 2017; pp. 1646–1651. [CrossRef]
4. Sedo, J.; Kascak, S. Control of single-phase grid connected inverter system. In Proceedings of the 2016 ELEKTRO, Strbske Pleso, Slovakia, 16–18 May 2016; pp. 207–212. [CrossRef]
5. Wu, H.; Wang, X. Design-Oriented Transient Stability Analysis of PLL-Synchronized Voltage-Source Converters. *IEEE Trans. Power Electron.* **2019**, *35*, 3573–3589. [CrossRef]
6. Fang, J.; Li, X.; Li, H.; Tang, Y. Stability Improvement for Three-Phase Grid-Connected Converters through Impedance Reshaping in Quadrature-Axis. *IEEE Trans. Power Electron.* **2017**, *33*, 8365–8375. [CrossRef]
7. Zhu, D.; Zhou, S.; Zou, X.; Kang, Y.; Zou, K. Small-Signal Disturbance Compensation Control for *LCL*-Type Grid-Connected Converter in Weak Grid. *IEEE Trans. Ind. Appl.* **2020**, *56*, 2852–2861. [CrossRef]
8. Yang, D.; Wang, X.; Liu, F.; Xin, K.; Liu, Y.; Blaabjerg, F. Symmetrical PLL for SISO Impedance Modeling and Enhanced Stability in Weak Grids. *IEEE Trans. Power Electron.* **2019**, *35*, 1473–1483. [CrossRef]
9. Zhu, D.; Zhou, S.; Zou, X.; Kang, Y. Improved Design of PLL Controller for *LCL*-Type Grid-Connected Converter in Weak Grid. *IEEE Trans. Power Electron.* **2019**, *35*, 4715–4727. [CrossRef]
10. Zhou, J.Z. Impact of short circuit ratio and phase locked loop parameters on the small-signal behaviour of a VSC-HVdc converter. In Proceedings of the 2016 IEEE Power and Energy Society General Meeting (PESGM), Boston, MA, USA, 17–21 July 2016; p. 1. [CrossRef]

11. Wu, X.; Huang, T.; Chen, X.; Hu, H.; He, G. Frequency Characteristic and Impedance Analysis on Three-Phase Grid-Connected Inverters Based on DDSRF-PLL. In Proceedings of the 2019 10th International Conference on Power Electronics and ECCE Asia (ICPE 2019—ECCE Asia), Busan, Korea, 27–31 May 2019. [CrossRef]
12. Scoltock, J.; Geyer, T.; Madawala, U.K. Model Predictive Direct Power Control for Grid-Connected NPC Converters. *IEEE Trans. Ind. Electron.* **2015**, *62*, 5319–5328. [CrossRef]
13. Zhang, L.; Harnefors, L.; Nee, H.-P. Power-Synchronization Control of Grid-Connected Voltage-Source Converters. *IEEE Trans. Power Syst.* **2009**, *25*, 809–820. [CrossRef]
14. Sun, Y.; Li, S. Comparison of conventional and a novel direct-current vector control for a LCL-filter based VSC-converter connected to weak grid. In Proceedings of the 2016 IEEE Power and Energy Society General Meeting (PESGM), Boston, MA, USA, 17–21 July 2016; pp. 1–5. [CrossRef]
15. Li, Z.; Yang, L.; Yang, D.; Peng, Z.; Shao, D.; Liu, J. Indirect Current Control Method Based on Reference Current Compensation of an LCL-Type Grid-Connected Inverter. *Energies* **2022**, *15*, 965. [CrossRef]
16. Agorreta, J.L.; Borrega, M.; López, J.; Marroyo, L. Modeling and Control of N -Paralleled Grid-Connected Inverters with LCL Filter Coupled Due to Grid Impedance in PV Plants. *IEEE Trans. Power Electron.* **2010**, *26*, 770–785. [CrossRef]
17. Wang, X.; Ruan, X.; Liu, S.; Tse, C.K. Full Feedforward of Grid Voltage for Grid-Connected Inverter with LCL Filter to Suppress Current Distortion Due to Grid Voltage Harmonics. *IEEE Trans. Power Electron.* **2010**, *25*, 3119–3127. [CrossRef]
18. Rodriguez, P.; Pou, J.; Bergas, J.; Candela, J.I.; Burgos, R.P.; Boroyevich, D. Decoupled Double Synchronous Reference Frame PLL for Power Converters Control. *IEEE Trans. Power Electron.* **2007**, *22*, 584–592. [CrossRef]
19. Rodríguez, P.; Luna, A.; Candela, I.; Mujal, R.; Teodorescu, R.; Blaabjerg, F. Multiresonant Frequency-Locked Loop for Grid Synchronization of Power Converters under Distorted Grid Conditions. *IEEE Trans. Ind. Electron.* **2010**, *58*, 127–138. [CrossRef]
20. Zhang, Z.; Gercek, C.; Renner, H.; Reinders, A.; Fickert, L. Resonance Instability of Photovoltaic E-Bike Charging Stations: Control Parameters Analysis, Modeling and Experiment. *Appl. Sci.* **2019**, *9*, 252. [CrossRef]
21. Golestan, S.; Guerrero, J.M.; Vidal, A.; Yepes, A.G.; Doval-Gandoy, J.; Freijedo, F.D. Small-Signal Modeling, Stability Analysis and Design Optimization of Single-Phase Delay-Based PLLs. *IEEE Trans. Power Electron.* **2015**, *31*, 3517–3527. [CrossRef]
22. Liserre, M.; Teodorescu, R.; Blaabjerg, F. Stability of photovoltaic and wind turbine grid-connected inverters for a large set of grid impedance values. *IEEE Trans. Power Electron.* **2006**, *21*, 263–272. [CrossRef]
23. Strachan, N.P.W.; Jovcic, D. Stability of a Variable-Speed Permanent Magnet Wind Generator with Weak AC Grids. *IEEE Trans. Power Deliv.* **2010**, *25*, 2779–2788. [CrossRef]
24. Wang, X.; Ruan, X.; Bao, C.; Pan, D.; Xu, L. Design of the PI regulator and feedback coefficient of capacitor current for grid-connected inverter with an LCL filter in discrete-time domain. In Proceedings of the 2012 IEEE Energy Conversion Congress and Exposition (ECCE), Raleigh, NC, USA, 15–20 September 2012; pp. 1657–1662. [CrossRef]